Design of Posterior Lumbar Fusion Internal Fixation Screws

Yuan Gao, Xiaoxuan Jiang, Li Wu*

Institute of Mechanical Engineering, Dalian Jiaotong University, Dalian 116028, China

Abstract: Posterior lumbar interbody fusion (PLIF) is a classic lumbar fusion procedure in spine surgery. The internal fixation screws used in the fusion procedure are the key components that are used to fix the vertebrae to the fusion device. Based on CT slice data and human anatomy theory, the finite element model (FEM) of the L1-L5 lumbar region was reconstructed using the principle of reverse engineering. Taking the L3 segment vertebral body model as an example, the screw insertion plan during the operation was determined. Then, the finite element model of screw extraction was established using the finite element software. The fixation effect of the pedicle screw embedded in the vertebral body was discussed through the finite element analysis method and orthogonal experiments, as well as the factors influencing the fixation effect of the screw. The results show that the contact area between the internal fixation screws of intervertebral fusion surgery and the cortical bone has a significantly greater impact on the fixation strength than the contact area with the cancellous bone. Choosing screws with a higher pitch and a larger outer diameter can significantly enhance their fixation effect. After considering various influencing factors comprehensively. The preferred size of the screw is an outer diameter of 6.0 mm, a pitch of 1.75 mm, and an SSA angle of 0°. This provides a basis for the design of intervertebral fusion internal fixation screws and the insertion method.

Keywords: Intervertebral Fusion; Pedicle Screw; Internal Fixation; Finite Element Analysis

DOI: 10.57237/j.wjcm.2025.01.002

1 Introduction

In recent years, the prevalence of lumbar degenerative diseases has steadily increased and gradually tended to be younger [1]. Interbody fusion has become an effective treatment for such diseases [2].

In order to improve the stability of the fusion, the arch-vertebral root screws and other internal fixation devices must be implanted into the human body together with the fusion cage during the PLIF fusion procedure [3]. Luo [4] et al. showed in a study that the stress of the internal fixation device was mainly concentrated in the screw and rod parts at both ends, and the stability of the vertebral body could be better maintained by using long-segment fixation. Lu et al. found that long arm uniaxial pedicle screw percutaneous approach achieved good results in the treatment of thoracolumbar spine [5], and the oblique lateral interbody fusion combined with bilateral pedicle screw fixation was not only feasible and accurate, but also significantly improved surgical efficiency and saved costs [6]. Lv and Li et al. used finite element analysis to study the biomechanical properties of the new transcredicular transdiscal (TPTD) screw fixation of the lumbar spine and the use of CBT screws to further achieve greater integration with the vertebrae, thereby reducing the risk of screw loosening [7, 8].

Although the current screw-rod system can maintain a certain degree of biomechanical properties, it has the dis-

Funding: Natural Science Foundation of Liaoning Province (Grant No. LJKMZ20220841).

*Corresponding author: Li Wu, djtuwuli@163.com

Received: 27 April 2025; Accepted: 9 July 2025; Published Online: 1 August 2025 http://www.wjclinmed.com

advantages of many consumables, large wound, and easy screw loosening. Therefore, this paper proposes a posterior oblique fixation screw, which can enhance the stability of the interbody fusion cage internal fixation system.

2 3D Model of Lumbar

The subject of this study was a 29-year-old healthy male volunteer with no history of lumbar spine trauma or congenital lumbar deformity. The initial lumbar spine model was extracted from the CT data by Mimics19.0 software and imported into GeomagicWrap2017 for surface optimization. The intervertebral disc, nucleus pulposus and articular cartilage models were drawn by 3-Matic software, and finally imported into the Creo7.0 assembly to obtain the complete geometric model, as shown in Figure 1. The model contained the following anatomical structures: four pairs of articular cartilage; Five vertebral bodies (each containing the upper and lower endplates, cancellous bone and cortical bone); Four intervertebral discs (composed of annulus fibrosus and nucleus pulposus) and seven groups of ligaments (including anterior longitudinal ligament, posterior longitudinal ligament, ligamentum flavum, transverse ligament, interspinous ligament, supraspinous ligament and facet ligament) [9] were fabricated in Hypermesh14.0. Table 1 lists the material parameters of the finite element model of lumbar L1-L5 segments [10-14].

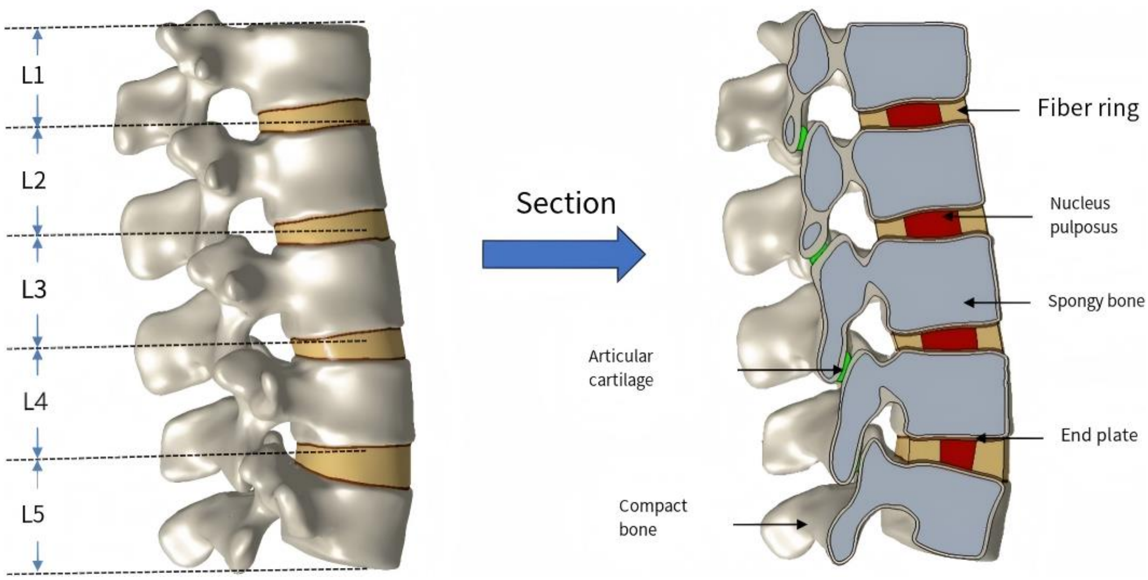

Figure 1 Geometric model of complete lumbar L1-L5 segment

Table 1 Material parameters of finite element model of lumbar L1-L5 segments

Model	**Modulus of elasticity (MPa)**	**Poisson's ratio**	**Density (kg/mm^3)**	**Cross-sectional area (mm^2)**
Cortical bone	12000	0.3	1.83×10^{-6}	/
Cancellous bone	100	0.2	1.70×10^{-7}	/
Plate of end	500	0.25	1.20×10^{-6}	/
Annulus fibrosus	4.2	0.45	1.05×10^{-6}	/
Nucleus pulposus	Hyperelastic, Mooney-Rivlin; C_{10}=0.12, C_{01}=0.03		1.02×10^{-6}	/
Articular cartilage	24	0.4	1.00×10^{-6}	/
Anterior longitudinal ligament	7.8	/	1.00×10^{-6}	63.7
Posterior longitudinal ligament	10	/	1.00×10^{-6}	20
Ligamentum flavum	15	/	1.00×10^{-6}	40
Interspinous ligament	4.56	/	1.00×10^{-6}	30
Supraspinous ligament	8	/	1.00×10^{-6}	40
Intertransverse ligament	10	/	1.00×10^{-6}	1.8
Joint capsule ligament	7.5	/	1.00×10^{-6}	30

A reference point was set on the upper surface of L1, at which a vertical 150 N axial compression force and 10 N·m torque (±Rx, ±Ry, ±Rz) in all directions were applied [15]. The total segmental ROM of the model under flexion, extension, left and right bending, and axial rotation was 14.123°, 10.527°, 10.639°, 10.812°, 7.211° and 7.242°, which was consistent with the variation trend of Yamamoto [16] and Chen [17] et al. The validity of the model was confirmed.

3 Design of Pedicle Screw and Screw Insertion Scheme

The stability of internal fixation devices of screw-rod system mainly depends on the holding force of the interface between vertebral body and screw, and the maximum axial pull-out strength test is the gold standard for evaluating the holding force of screw. This method objectively reflects the binding strength by recording the load-displacement curve and measuring the ultimate pull-out load [18].

3.1 Determination of Entry Point of Pedicle Screw

As the starting point of the screw trajectory, the entry point directly determines the direction of the screw in the three-dimensional space of the vertebral body [19]. According to the sectional image measurement results of CT data, the insertion point was determined by the Magerl method, as shown in Figure 2.

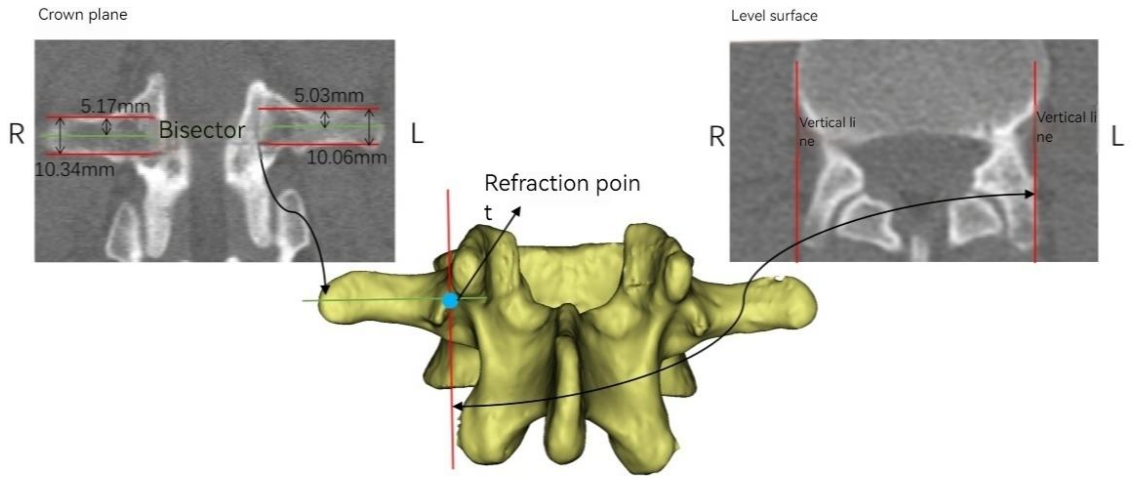

Figure 2 Schematic diagram of the Magerl entry point at lumbar L3 segment

3.2 Determination of Pedicle Screw Insertion Angle

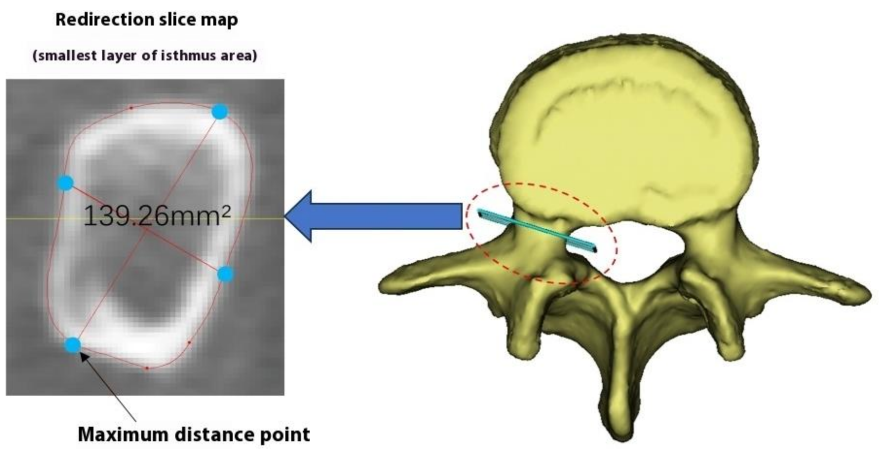

Figure 3 Reorientation of left pedicle isthmus at lumbar L3 segment

The lumbar pedicle isthmus is the narrowestern anatomical bottleneck [20], and its cross-sectional area determines the safety boundary of screw implantation. As shown in Figure 3, using the Reslice function in Mimics19.0, the CT sectional image was redirected, and the area of the vertebral arch root position in the image of each reorientation layer was measured to determine the isthmus, and then the widest and highest position point was found.

By constructing the spatial connection between the entry point and the widest and highest point, and projecting it to the horizontal and sagittal planes for Angle measurement, the three-dimensional insertion Angle range of the pedicle screw in the insertion scheme can be determined. The SSA Angle ranged from 5.58 °to 30.70 °in the horizontal plane and from -28.42 °to 11.09 °in the sagittal plane (TSA Angle was positive when the head of the screw was tilted into the vertebral body, and negative otherwise; The SSA Angle parallel to the upper and lower endplates was defined as 0 °). Due to the small allowable variation range of the TSA Angle of screw placement and the thin thickness of the cortical bone on the inner and outer sides of the pedicle, the SSA Angle was selected as the design variable in this paper, and the values were -10 °, 0 °, and 5 °, respectively. The TSA Angle was 16 °as quantitative for subsequent studies.

3.3 Establishment of the Screw Model

The influence of screw diameter and pitch on the effect of internal fixation was explored. The screw diameter was set at 5.0 mm, 5.5 mm and 6.0 mm, the pitch was set at 1.75 mm, 1.75 mm-3.00 mm and 3.00-1.75 mm, and the screw length was defined as 50 mm. The screws were modeled in Creo7.0, and a set of models with a constant diameter and a changed pitch is shown in Figure 4. The screw threads were designed according to the national medical industry standard YY0018 -- 2016, which were P=1.75 mm, e=0.1 mm, α=35 °, β=3 °, r_4=1.0 mm and r_5=0.3 mm.

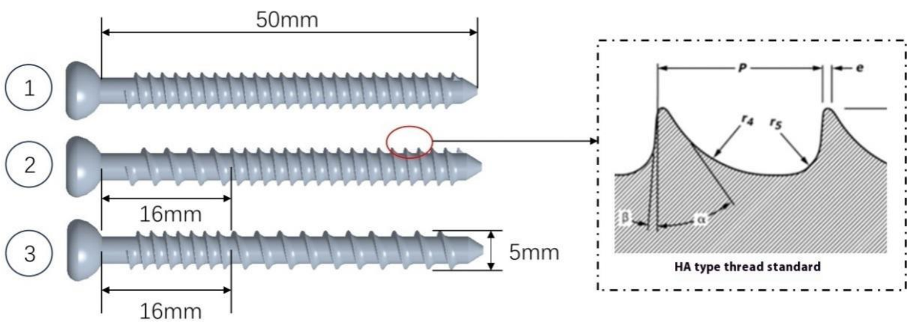

Figure 4 The 5mm diameter pedicle screw group and its dimensions

3.4 Design of Orthogonal Test

The screw diameter, pitch and SSA Angle were set as variables, and the screw length, thread, Magerl insertion point and insertion depth of 45 mm were set as quantitative parameters. An orthogonal test scheme with three factors and three levels was designed, as shown in Table 2.

Table 2 Orthogonal experimental design

Serial number	Outer diameter (mm)	Pitch (mm)	SSA Angle (°)
1	5.0	1.75	0
2	5.0	3.00~1.75	-10
3	5.0	1.75~3.00	5
4	5.5	1.75	-10
5	5.5	3.00~1.75	5
6	5.5	1.75~3.00	0
7	6.0	1.75	5
8	6.0	3.00~1.75	0
9	6.0	1.75~3.00	-10

4 Analysis of Influencing Factors of Pedicle Screw Fixation

The finite element analysis method was used to simulate the pullout effect of pedicle screw in the vertebra, and the maximum pullout force in nine orthogonal test schemes was obtained, so as to discuss the influencing factors and provide theoretical basis for the design of a new type of pedicle screw.

4.1 Finite Element Model for Screw Pull-out

According to the preset screw insertion parameters, the finite element model was assembled with the L3 vertebral body model, and the unilateral pedicle screw path was generated by Boolean operation to complete the geometric modeling of screw placement under the composite structure of cortical bone and cancellous bone. The model of the first set of tests is shown in Figure 5 (a).

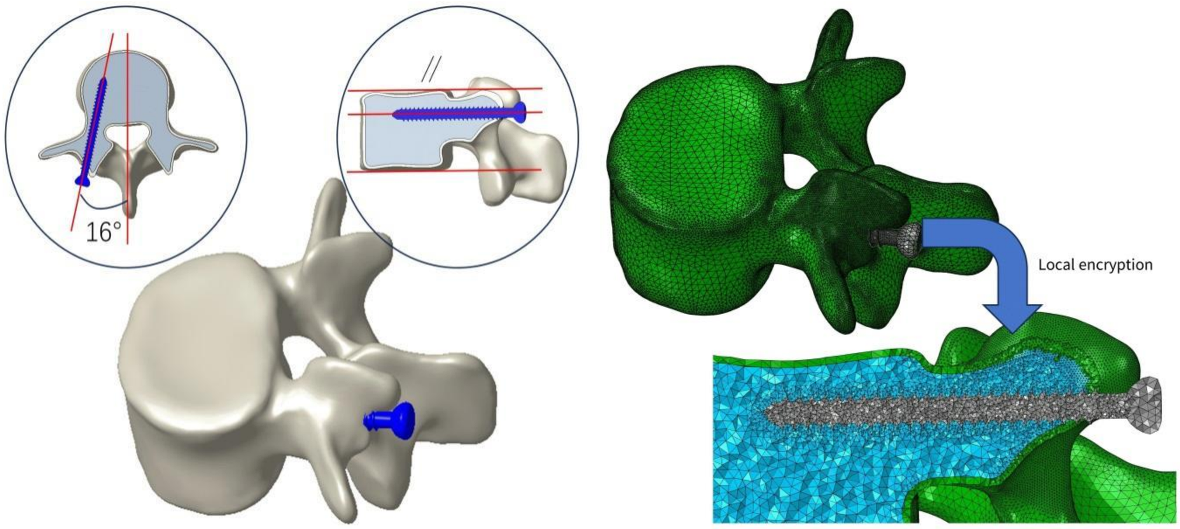

(a) (b)

Figure 5 Geometric model (a) and finite element model (b) of screw implantation in the vertebral body

Then, the overall meshing of the finite element model was carried out in Hypermesh14.0. Among them, the mesh size of the vertebral body near the screw and the screw channel was defined as 0.4 mm, and the mesh size of the remaining parts of the vertebral body was set to 0.5 mm—2 mm. The model is divided into a total of 644,896 grids, and all the grid cell types are C3D4. The results are shown in Figure 5 (b).

The pedicle screw material adopts Ti-6Al-4V alloy material. Its elastic modulus is set at 110 GPa, Poisson's ratio is 0.3, and the mass density is 4.52×10^{-6} kg/mm^3.

The symmetrical elastoplastic material law (Johnson-Cook) was selected for the assignment of vertebral body materials, and it was allowed to calculate the Von Mises hardening with ductile damage until potential rupture occurred. The J-C model parameters of cortical bone and cancellous bone selected in this study are shown in Table 3 [21]:

Table 3 Parameters of J-C elastic-plastic constitutive model of vertebral body

Material properties	**Cortical bone**	**Cancellous bone**
Yield stress, A (MPa)	110	1.92
Strain hardening parameter, B (MPa)	100	20
Strain hardening rate, n	0.1	1

The inner surface of the cortical bone and the outer surface of the cancellous bone of the vertebral body were defined as binding constraints, and the outer surface of the screw and the inner surface of the vertebral body were defined as surface-to-surface contact. The tangential behavior was defined as penalty friction, and the coefficient was 0.2. Normal behavior is defined as hard contact and separation after contact is allowed [22]. The upper and lower surfaces of the vertebral body were completely fixed and their degrees of freedom were constrained in all directions. A coupling point RP-1 was set at the tail end of the screw, and a pull-out displacement along the axis of the screw was applied after coupling this point to the tail plane of the screw.

4.2 Simulation Results

The changes in the vertebral state during the screw extraction process of the first group of models are shown in Figure 6.

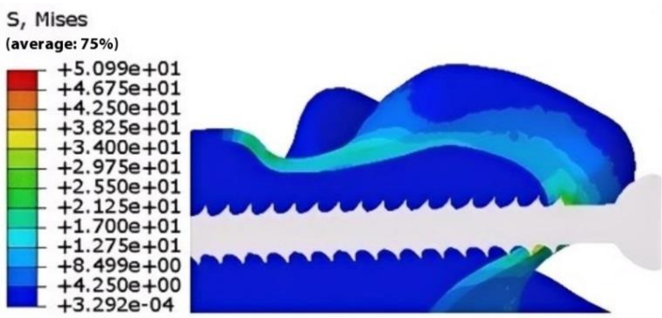

(a) Pull-out displacement 0.2mm

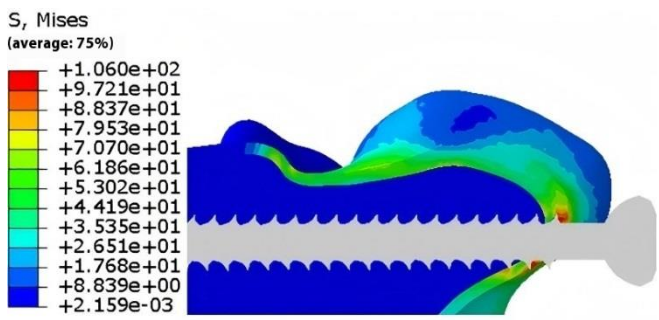

(b) Pull-out displacement 0.4mm

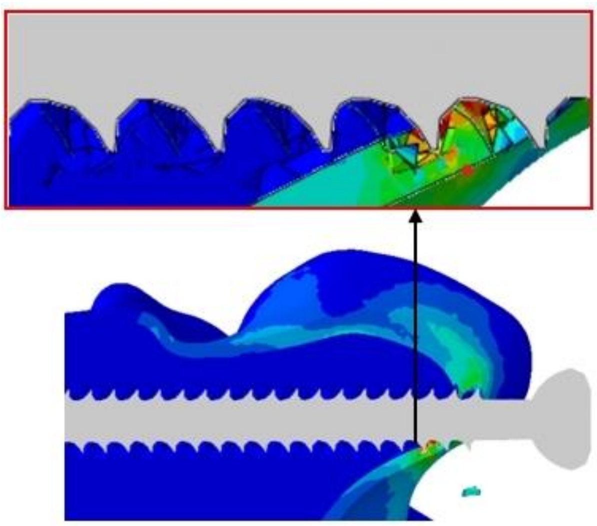

(c) Pull-out displacement 0.5mm

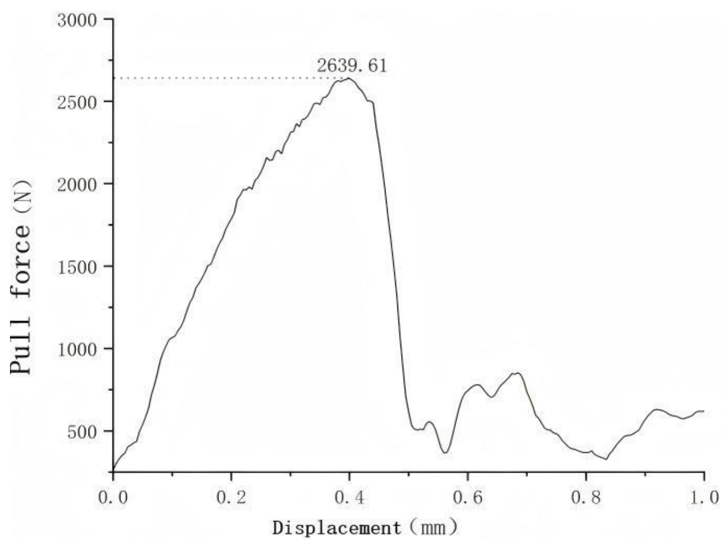

(d) Pull-out force - displacement curve

Figure 6 The vertebral body changes and the curves of extraction force and displacement during the extraction process of the first group of models

It can be seen from the above figure that during the screw extraction process, the maximum stress on the vertebra always appeared at the cortical bone site in contact with the tail of the screw. When the displacement of the screw was 0.2 mm, the maximum stress of the vertebral body was 50.99 MPa, which did not reach the yield strength of the cortical bone. When the screw pullout was 0.4 mm, the maximum stress of the cortical bone of the vertebral body increased to 106.0 MPa, which was close to the strength of the vertebral body, and the destruction of the vertebral body could be inferred. When the displacement continued to increase to 0.5 mm, the cortical bone and cancellous bone of the vertebral body appeared obvious damage, and the pullout force dropped from the maximum value of 2639.61 N to 628.35 N. At this time, it was judged that the screw fixation had failed.

According to the analysis process of the first group, the other eight groups of orthogonal tests were carried out, and the results of the maximum pull-out force were shown in Table 4. By comparing the nine groups of data, it can be seen that the maximum value of the maximum pull-out force appeared in the seventh group of models, and its value was 2963.31 N. However, the maximum pull-out force of the second group of models was the smallest, with a value of 1811.25 N. At the same time, in the process of simulated screw pullout, the models of each group all conformed to the same law: with the gradual increase of screw pullout displacement, the pullout force also increased. It can be further inferred that before the maximum pull-out force is reached, the pull-out force-displacement curve can be approximately linear, indicating that the vertebra is still in the linear elastic region at this time, and no permanent damage occurs. When the displacement continues to increase, the pull-out force curve shows a significant downward trend, and the vertebra will be destroyed until complete failure. This change rule of load displacement is consistent with the experimental results of Gao [23] et al., and then the validity of nine groups of experiments is verified.

Table 4 Maximum pull-out force

Orthogonal Experiment Group Number	Maximum pulling force (N)
1	2639.61
2	1811.25
3	1965.09
4	2857.46
5	2138.61
6	2264.09
7	2963.31
8	2239.41
9	2361.79

4.3 Analysis of Influencing Factors

The pull-out force results of the above nine groups of models were analyzed by the range analysis method to determine the primary and secondary relationship of the influence of various factors on the maximum pull-out strength of screws. The results are shown in Table 5.

Table 5 Maximum pull-out force range analysis table

Calculated value	Factors		
	Outer diameter of screw (mm)	Pitch of pitch (mm)	SSA Angle (°)
k_1	2138.65	2820.13	2381.04
k_2	2420.05	2063.09	2343.50
k_3	2521.50	2196.99	2355.67
Range R	382.85	757.04	37.54

By calculating the maximum values of k1, k2, and k3 under each factor, the best combination of factors could be judged as the screw external diameter of 6.0 mm, pitch of 1.75 mm, and SSA Angle of 0°, and the pullout strength of the model was the maximum. At the same time, by comparing the range value R under each factor, it can be seen that the primary and secondary order of influencing the maximum pull-out force of the screw is pitch > screw diameter > SSA Angle.

Further analysis shows that the change of screw pitch can be approximated to the change of contact area between screw and vertebral body. The smaller the pitch, the larger the contact area between screw and vertebral body, and the higher the pull-out strength [24]. By comparing the six groups of models with variable pitch (2 and 3, 5 and 6, 8 and 9), it was found that although the screw with small head pitch and large tail pitch had larger contact area with the vertebral bone, its maximum pullout force was smaller than that of the screw with large head pitch and small tail pitch. The main reason was that the tail end of the screw was in contact with the cortical bone of the vertebral body, and the tip was in contact with the cancellous bone. The elastic modulus of cortical bone is significantly higher than that of cancellous bone, which is more resistant to deformation and therefore can bear more loads [25]. Wu et al. found in their research that as the number of cortical bone layers in contact with the cortical bone trajectory screw increases, the axial pullout force also increases. Therefore, in clinical practice, it is hoped that the screw will be in contact with more than three layers of cortical bone to achieve higher screw implant stability. This increase in the number of contact layers further indicates that increasing the contact area between the screw and cortical bone can effectively enhance its stability [26]. Meanwhile, Hironobu et al.'s clinical controlled experiment on the cortical bone trajectory (CBT) screw technique also fully demonstrated that in the CBT group, hard bone bonding reached 90.9%, and it was less invasive to the bone [27], which also indicates that in terms of internal fixation effect, the contact area between the screw and cortical bone plays a significant role. Combining the above research, it is ultimately proposed that the size of the contact area between the screw and cortical bone has a more significant impact on the fixation strength than that between the screw and cancellous bone.

In terms of the selection principle of specific dimensions, Keitaro et al. analyzed 720 different diameters and lengths of CBT screws in 20 different lumbar vertebrae through the finite element method. They proposed that the screw diameter is an important factor affecting the strength of internal fixation, and the ideal screw size of CBT is a diameter greater than 5.5 mm and a length greater than 35 mm, which can be more conducive to the fixation strength of the vertebrae [28]. According to the fatigue tests of screws with different outer diameters on 10 human cadaveric vertebrae conducted by Lennart et al., it was concluded that increasing the screw diameter from the standard 6 mm to the possible maximum diameter (8 mm to 10 mm) would achieve higher structural stiffness [29]. Regarding the selection of pitch, Daud et al. constructed six different 3D pedicle screw models and compared the bending and pull-out force performance of different pedicle screws through the finite element analysis method. From the simulation results, it was found that the internal fixation screws with a denser pitch have better pull-out performance [30]. Based on the above studies, it can be concluded that when selecting the parameters of pedicle screws, a denser pitch and a larger outer diameter should be preferred in the design, which can significantly enhance the fixation effect.

5 Conclusions

Based on the finite element and orthogonal test method, it is concluded that the most important influencing factor of the internal fixation effect of pedicle screw is the pitch, followed by the outer diameter of the screw, and the last is the SSA Angle. The screw structure parameters and screw placement parameters are proposed, which can enhance the internal fixation effect and stability of the arch-vertebral root screw, improve the shortcomings of screw loosening, and improve the treatment effect of posterior lumbar interbody fusion.

References

[1] Ravindra V M, Senglaub S S, Rattani A, et al. Degenerative lumbar spine disease: estimating global incidence and worldwide volume [J]. Global spine journal, 2018, 8(8): 784-794. https://doi.org/10.1177/2192568218770769

[2] Eliasberg C D, Kelly M P, Ajiboye R M, et al. Complications and rates of subsequent lumbar surgery following lumbar total disc arthroplasty and lumbar fusion [J]. Spine, 2016, 41(2): 173-181. https://doi.org/10.1097/BRS.0000000000001180

[3] Mobbs R J, Phan K. History of retractor technologies for percutaneous pedicle screw fixation systems [J]. Orthopaedic surgery, 2016, 8(1): 3-10. https://doi.org/10.1111/os.12216

[4] Peijie L U O. Comparison of the short-segment and long-segment cement-augmented pedicle screw fixation for osteoporotic thoracolumbar fracture: a finite element study [J]. Chinese Journal of Tissue Engineering Research, 2020: 342-347. https://doi.org/10.3969/j.issn.2095-4344.1926

[5] Lu P, Pan T, Dai T, et al. Is unilateral pedicle screw fixation superior than bilateral pedicle screw fixation for lumbar degenerative diseases: a meta-analysis [J]. Journal of Orthopaedic Surgery and Research, 2018, 13: 1-13. https://doi.org/10.1186/s13018-018-1004-x

[6] Blizzard D J, Thomas J A. MIS single-position lateral and oblique lateral lumbar interbody fusion and bilateral pedicle screw fixation: feasibility and perioperative results [J]. Spine, 2018, 43(6): 440-446. https://doi.org/10.1097/BRS.0000000000002330

[7] Lv Q B, Gao X, Pan X X, et al. Biomechanical properties of novel transpedicular transdiscal screw fixation with interbody arthrodesis technique in lumbar spine: a finite element study [J]. Journal of orthopaedic translation, 2018, 15: 50-58. https://doi.org/10.1016/j.jot.2018.08.005

[8] Li X, Abdel-Latif K H A, Schwab J, et al. Biomechanical impact of cortical bone vs. traditional pedicle screw trajectories: a finite element study on lumbar spinal instrumentation [J]. Frontiers in Bioengineering and Biotechnology, 2025, 13: 1541114. https://doi.org/10.3389/fbioe.2025.1541114

[9] Wu L, Jiang X, Guan T, et al. Biomechanical properties analysis of posterior lumbar interbody fusion with transpedicular oblique screw fixation, [J]. Heliyon, 2024, 10(19): e38929-e38929. https://doi.org/10.1016/j.heliyon.2024.e38929

[10] Ding H, Liao L, Yan P, et al. Three-Dimensional Finite Element Analysis of L4-5 Degenerative Lumbar Disc Traction under Different Pushing Heights [J]. Journal of Healthcare Engineering, 2021, 2021(1): 1322397. https://doi.org/10.1155/2021/1322397

[11] Huang S F, Chang C M, Liao C Y, et al. Biomechanical evaluation of an osteoporotic anatomical 3D printed posterior lumbar interbody fusion cage with internal lattice design based on weighted topology optimization [J]. International Journal of Bioprinting, 2023, 9(3): 697. https://doi.org/10.18063/ijb.697

[12] Kahaer A, Zhang R, Wang Y, et al. Hybrid pedicle screw and modified cortical bone trajectory technique in transforaminal lumbar interbody fusion at L4-L5 segment: finite element analysis [J]. BMC Musculoskeletal Disorders, 2023, 24(1): 288. https://doi.org/10.1186/s12891-023-06385-y

[13] Fan W, Guo L X, Zhang M. Biomechanical analysis of lumbar interbody fusion supplemented with various posterior stabilization systems [J]. European Spine Journal, 2021, 30(8): 2342-2350. https://doi.org/10.1007/s00586-021-06856-7

[14] Hangkai S, Yuru C, Zhenhua L, et al. Biomechanical evaluation of anterior lumbar interbody fusion with various fixation options: Finite element analysis of static and vibration conditions [J]. Clinical Biomechanics, 2021, 84: 105339-105339. https://doi.org/10.1016/j.clinbiomech.2021.105339

[15] Zhang Q, Chon T E, Zhang Y, et al. Finite element analysis of the lumbar spine in adolescent idiopathic scoliosis subjected to different loads [J]. Computers in biology and medicine, 2021, 136: 104745. https://doi.org/10.1016/j.compbiomed.2021.104745

[16] Yamamoto I, Panjabi M M, Crisco T, et al. Three-dimensional movements of the whole lumbar spine and lumbosacral joint [J]. Spine, 1989, 14(11): 1256-1260. https://doi.org/10.1097/00007632-198911000-00020

[17] Chen C S, Cheng C K, Liu C L, et al. Stress analysis of the disc adjacent to interbody fusion in lumbar spine [J]. Medical engineering & physics, 2001, 23(7): 485-493. https://doi.org/10.1016/S1350-4533(01)00076-5

[18] Tsai Y Y, Hsieh M K, Lai P L, et al. Predicting pullout strength of pedicle screws in broken bones from X-ray images [J]. Journal of the Mechanical Behavior of Biomedical Materials, 2022, 134: 105366. https://doi.org/10.1016/j.jmbbm.2022.105366

[19] Doğu H. The Optimal Entry Point and Trajectory for Pedicle Screws to Avoid Superior Facet Joint Violation and Pedicle Penetration [J]. Cureus, 2024, 16(10). https://doi.org/10.7759/cureus.72719

[20] Raasck K, Khoury J, Aoude A, et al. The effect of thoracolumbar pedicle isthmus on pedicle screw accuracy [J]. Global Spine Journal, 2020, 10(4): 393-398. https://doi.org/10.1177/2192568219850143

[21] El-Rich M, Arnoux P J, Wagnac E, et al. Finite element investigation of the loading rate effect on the spinal load-sharing changes under impact conditions [J]. Journal of biomechanics, 2009, 42(9): 1252-1262. https://doi.org/10.1016/j.jbiomech.2009.03.036

[22] Hang Z Q, Huat T S, Meng C S. Effects of bone materials on the screw pull-out strength in human spine [J]. Medical Engineering & Physics, 2006, 28(8): 795-801. https://doi.org/10.1016/j.medengphy.2005.11.009

[23] Gao M, Lei W, Wu Z, et al. Biomechanical evaluation of fixation strength of conventional and expansive pedicle screws with or without calcium based cement augmentation [J]. Clinical Biomechanics, 2011, 26(3): 238-244. https://doi.org/10.1016/j.clinbiomech.2010.10.008

[24] Tintara H, Aiyarak P, Mitarnun W, et al. Effect of thread pitch on pull-out strength of laparoscopic myoma screws [J]. Journal of Obstetrics and Gynaecology Research, 2006, 32(4): 428-433. https://doi.org/10.1111/j.1447-0756.2006.00427.x

[25] Sahi A, Gali S. Effect of implant systems in differing bone densities on peri-implant bone stress: a 3 dimensional finite element analysis [J]. Materials Today: Proceedings, 2022, 50: 1300-1307. https://doi.org/10.1016/j.matpr.2021.08.231

[26] Wu C, Long H, Fu Y, et al. Finite Element Analysis of Cortical Bone Trajectory Screw Resistance to Pullout During Exposure to Different Cortical Layers Based on AbaqusCEA Software [J]. Indian Journal of Orthopaedics, 2023, 57(8): 1329-1337. https://doi.org/10.1007/s43465-023-00944-0

[27] Sakaura H, Miwa T, Yamashita T, et al. Cortical bone trajectory screw fixation versus traditional pedicle screw fixation for 2-level posterior lumbar interbody fusion: comparison of surgical outcomes for 2-level degenerative lumbar spondylolisthesis [J]. Journal of Neurosurgery: Spine, 2017, 28(1): 57-62. https://doi.org/10.3171/2017.5.spine161154

[28] Matsukawa K, Yato Y, Imabayashi H, et al. Biomechanical evaluation of fixation strength among different sizes of pedicle screws using the cortical bone trajectory: what is the ideal screw size for optimal fixation? [J]. Acta neurochirurgica, 2016, 158: 465-471. https://doi.org/10.1007/s00701-016-2705-8

[29] Viezens L, Sellenschloh K, Püschel K, et al. Impact of screw diameter on pedicle screw fatigue strength—A biomechanical evaluation [J]. World neurosurgery, 2021, 152: e369-e376. https://doi.org/10.1016/j.wneu.2021.05.108

[30] Daud R, Kae W Y, Ayu H M, et al. Effect of thread profile variation on pullout and bending strength of a pedicle screw [C] // IOP Conference Series: Materials Science and Engineering. IOP Publishing, 2021, 1078(1): 012025. https://doi.org/10.1088/1757-899x/1078/1/012025